



# Lifetime measurement of excited states in $^{116}\text{Xe}$

Casper-David Lakenbrink<sup>1,a</sup>, Marcel Beckers<sup>1</sup>, Andrey Blazhev<sup>1</sup>, Alfred Dewald<sup>1</sup>, Felix Dunkel<sup>1</sup>, Arwin Esmaylzadeh<sup>1</sup>, Christoph Fransen<sup>1</sup>, Jan Jolie<sup>1</sup>, Lukas Knafila<sup>1</sup>, Claus Müller-Gatermann<sup>2</sup>, Franziskus von Spee<sup>1</sup>, Karl-Oskar Zell<sup>1</sup>

<sup>1</sup> Institut für Kernphysik, Universität zu Köln, Zùlpicher Str. 77, Cologne 50937, Germany

<sup>2</sup> Physics Division, Argonne National Laboratory, 9700 South Cass Avenue, Lemont, IL 60439, USA

Received: 25 August 2023 / Accepted: 25 November 2023

© The Author(s) 2023

Communicated by Wolfram Korten

**Abstract** Lifetimes of excited states in  $^{116}\text{Xe}$  were measured using the recoil-distance Doppler-shift technique. Excited  $^{116}\text{Xe}$  nuclei were populated in the fusion-evaporation reaction  $^{102}\text{Pd}(^{16}\text{O},2n)^{116}\text{Xe}$ . Lifetimes of the  $2_1^+$  and  $4_1^+$  states were evaluated using the differential decay-curve method with  $\gamma$ - $\gamma$ -coincidence data as well as lifetimes of the  $6_1^+$  and  $7_1^-$  states using simulations of spectra considering Doppler-shift attenuation effects.

## 1 Introduction

Previous measurements of transition strengths in the neutron-deficient even-even Te and Xe nuclei have unveiled an interesting behavior. Following the  $N_\pi N_\nu$  scheme [1], an increase in the reduced transition strength of the ground state transition,  $B(E2; 2_1^+ \rightarrow 0_1^+)$ , is expected from the shell closures at  $N = 50$  and  $N = 82$  towards neutron mid-shell. This behavior is qualitatively very well reproduced by the experimental data for the Te and Xe isotopes, as can be seen in Fig. 1.

For further information on the nuclear structure, the ratio  $B_{4/2} = B(E2; 4_1^+ \rightarrow 2_1^+)/B(E2; 2_1^+ \rightarrow 0_1^+)$  is a key observable (see, for example, Ref. [45]). For nuclei far away from closed shells, a collective behavior is expected, indicated by a  $B_{4/2}$  ratio in between the value of a rotor ( $B_{4/2} \approx 1.43$ ) and a vibrator ( $B_{4/2} = 2$ ). Typically, nuclei at mid-shell for both protons and neutrons are expected to be deformed and thus show a rotor-like behavior, while nuclei closer to the shell closures are expected to behave vibrator-like. Any  $B_{4/2}$  ratio outside this range can not be explained with a collective model. Especially ratios  $\lesssim 1$  are usually interpreted as indicators for a non-collective behavior or shape coexistence as discussed in, e.g., Ref. [46].

In Fig. 2 the  $B_{4/2}$  ratios for the Xe and Te isotopes are shown. While it is not surprising that the very simple collective approach can not perfectly describe the Te and Xe isotopes lying close in  $Z$  to the magic Sn nuclei, the values of  $B_{4/2} \lesssim 1$  in nuclei near neutron mid-shell and the non-smooth behavior are still very surprising. It can be seen in Fig. 2 that the  $B_{4/2}$  ratios for  $^{114}\text{Xe}$  [2, 3] and  $^{114}\text{Te}$  [4] have been measured to be  $< 1$ . A comparison with the Te isotopes is made difficult by the fact that for  $^{116}\text{Te}$  no  $B_{4/2}$  ratio is known, which would be a crucial data point neighboring the nucleus  $^{114}\text{Te}$  with  $B_{4/2} < 1$ .

In the Sn isotopic chain, a similar behavior can be seen exhibiting a drop in  $B_{4/2}$  ratios between  $^{116}\text{Sn}$  and  $^{114}\text{Sn}$  with values of  $B_{4/2} \lesssim 1$  for  $^{108-114}\text{Sn}$ . Unlike in the Te and Xe isotopes however, this is not only due to a lowering of the  $B(E2; 4_1^+ \rightarrow 2_1^+)$  values, but also an increase in  $B(E2; 2_1^+ \rightarrow 0_1^+)$  values (see Fig. 1 in Ref. [5]). The latter could be explained with Monte Carlo shell model calculations in Ref. [48]. In these calculations, an increase in  $B(E2; 2_1^+ \rightarrow 0_1^+)$  strengths from  $^{116}\text{Sn}$  towards lower neutron numbers is explained by the number of proton holes in the  $1g_{9/2}$  orbit. The breaking of the magic  $Z = 50$  core and excitation of protons from the  $1g_{9/2}$  to the  $2d_{5/2}$  orbit are associated with a stronger quadrupole deformation caused by the proton-neutron interaction [48]. For the lowering of the  $B(E2; 4_1^+ \rightarrow 2_1^+)$  values, however, no conclusive theoretical explanation exists for the Sn, Te or Xe isotopes. While the increase in  $B(E2; 2_1^+ \rightarrow 0_1^+)$  strengths seems to be limited to the semi-magic Sn nuclei, the decrease in  $B(E2; 4_1^+ \rightarrow 2_1^+)$  strengths seems to represent an unexpected structural change that appears also in the Te and Xe nuclei.  $^{116}\text{Xe}$  is in this regard a key nucleus as the current data suggest a sharp drop of the  $B_{4/2}$  ratios between  $^{116}\text{Xe}$  and  $^{114}\text{Xe}$ .

The only previous evaluation of transition strengths in  $^{116}\text{Xe}$  was performed in a lifetime measurement employing

<sup>a</sup> e-mail: clakenbrink@ikp.uni-koeln.de (corresponding author)

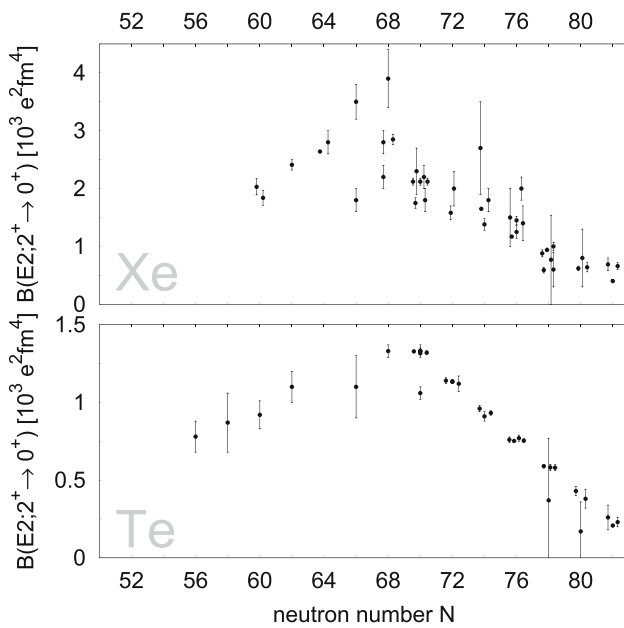


**Fig. 1** Evolution of  $B(E2; 2_1^+ \rightarrow 0_1^+)$  values for the even Te, Xe isotopes between the shell closures at  $N=50$  and  $N=82$ . Different values for the same neutron number have been slightly shifted horizontally to sustain readability. Experimental data taken from Refs. [2–44]

the recoil-distance Doppler-shift (RDDS) technique [2]. The lifetimes were analyzed from  $\gamma$ -ray singles spectra for which the relative feeding intensities and lifetimes of all feeding states—direct as well as indirect feeding—have to be taken into account. Especially in the case of fusion-evaporation reactions like the one used in Ref. [2], the feeding history is usually complex and the higher-lying states are often populated to a significant fraction via unobserved feeding. For this unobserved feeding, an effective lifetime has to be assumed, which is derived from the same fit as the lifetimes of interest, resulting in a larger number of degrees of freedom. Thus an analysis in singles spectra is prone to errors in the accounting of feeding.

In this work, lifetimes in  $^{116}\text{Xe}$  were also evaluated from an RDDS experiment. For the lifetime analysis of the  $2_1^+$  and  $4_1^+$  states, the differential decay-curve method (DDCM) with data from  $\gamma$ - $\gamma$ -coincidence matrices was used for the first time in this nucleus. By setting  $\gamma$  gates on the shifted component of a directly feeding transition, the necessity for any assumptions on feeding conditions can be eliminated as described in Ref. [49]. Furthermore, when applying the DDCM, only relative target-to-stopper distances are needed, which can be measured far more precisely than absolute distances. The level lifetimes of the  $6_1^+$  and  $7_1^-$  states were also evaluated using simulations of spectra considering Doppler-shift attenuation effects, since the lifetime results from a DDCM analysis were of the order of the stopping time of the recoiling nuclei.

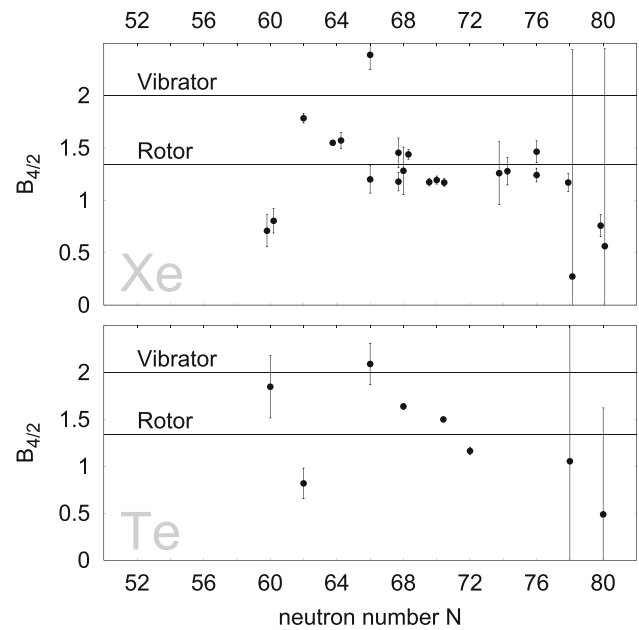


**Fig. 2** Evolution of  $B_{4/2} = B(E2; 4_1^+ \rightarrow 2_1^+) / B(E2; 2_1^+ \rightarrow 0_1^+)$  values for the even Te, Xe isotopes between the shell closures at  $N = 50$  and  $N = 82$ . Different values for the same neutron number have been slightly shifted horizontally to sustain readability. The values for the collective models of the rotor and vibrator are marked. Experimental data taken from Refs. [2–5, 8–10, 19, 22–28, 30, 33–35, 38, 39, 41, 42, 47]

## 2 Experimental setup

The RDDS experiment to measure lifetimes in  $^{116}\text{Xe}$  was conducted at the FN-tandem accelerator at the University of Cologne, Germany, using the Cologne coincidence plunger device [49]. Excited states in  $^{116}\text{Xe}$  were populated in the fusion-evaporation reaction  $^{102}\text{Pd}(^{16}\text{O}, 2n)^{116}\text{Xe}$  at a beam energy of 62 MeV. The  $^{102}\text{Pd}$  target foil had a thickness of 1.0 mg/cm<sup>2</sup> with an enrichment of 69%. A Ta foil with a thickness of 3.1 mg/cm<sup>2</sup> was used to stop the recoiling nuclei. For detection of  $\gamma$  rays, 11 high-purity germanium (HPGe) detectors were used arranged in two rings at angles of 45° (ring 1, 6 detectors) and 142.3° (ring 2, 5 detectors) with respect to the beam axis. The measurement was performed at ten different target-to-stopper distances ranging from 1  $\mu\text{m}$  to 150  $\mu\text{m}$  with respect to the electrical contact point between the target and stopper foils. Fluctuations in the distance were compensated by an automatic feedback control system using the capacitance between the two foils as a measure for the distance.

## 3 Data analysis and results

For the analysis, the data from the HPGe detectors were sorted in  $\gamma$ - $\gamma$ -coincidence matrices using the sort code SOCOv2 [50]. The matrices were sorted ring-wise giving

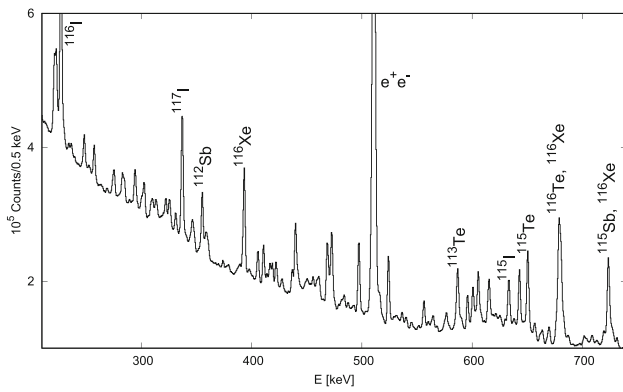


**Fig. 3** Projection of the  $\gamma$ - $\gamma$  matrix 1\_1 for 1  $\mu\text{m}$  distance. For each of the strong channels of the fusion-evaporation reaction, the  $\gamma$  peak with the highest intensity is labeled. Also the  $e^+e^-$ -annihilation line is labeled. The non-labeled peaks correspond to less intense  $\gamma$  transitions in the reaction products. The background mostly consists of Compton background

four possible ring-ring combinations N\_M where the gate is set on events in ring M and the resulting spectrum shows coincident events in ring N. A projection of the  $\gamma$ - $\gamma$  matrix 1\_1 for a target-to-stopper distance of 1  $\mu\text{m}$  can be seen in Fig. 3. Since other reaction channels are also populated with large cross sections, it is very difficult and for some transitions even impossible to avoid contaminations in the  $\gamma$  gates. These contaminations however, are only a problem if they have a coincident transition with a similar energy as the transition of interest. Thus it is very important to carefully check for any contaminations and their coincident transitions that may appear in a gated spectrum. To give an impression of the available  $\gamma$ -ray statistics per distance in the gated spectra, a spectrum resulting from a gate on both components of the  $2_1^+ \rightarrow 0_1^+$  transition in  $^{116}\text{Xe}$  for the 1  $\mu\text{m}$  distance can be seen in Fig. 4.

For the lifetime analysis, the differential decay-curve method (DDCM) was used in  $\gamma$ - $\gamma$ -coincidence mode as described in Ref. [49]. It has the advantages that only relative target-to-stopper-distances are needed, which can be measured far more precisely than absolute distances, and that no assumptions on feeding conditions are needed. To determine the lifetime of a state, a gate was set on the Doppler-shifted component of a feeding transition. In the resulting spectrum, the Doppler-shifted and unshifted components of a depopulating  $\gamma$ -ray transition were fitted by Gaussian functions. For very small and very large distances, the intensity of one of the two peaks is very small. To ensure a reliable fit of the peak intensities also for these distances, the degrees of freedom in the fit were reduced by fixing the peak width and position. The lifetime for the measurement at distance  $x$  was then deduced from the intensities of the shifted/unshifted component  $I_{\text{sh/un}}$

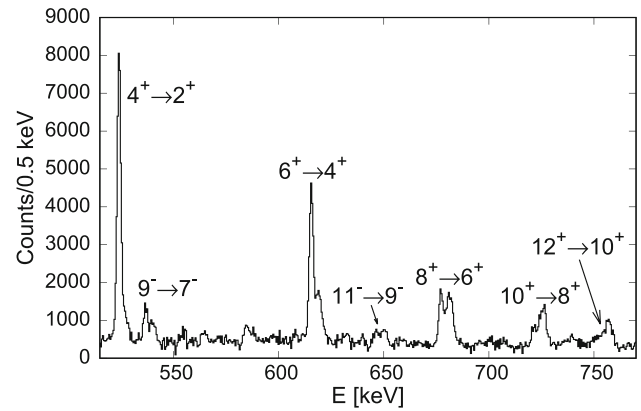


**Fig. 4**  $\gamma$ -ray spectrum resulting from a gate on both components of the  $2_1^+ \rightarrow 0_1^+$  transition in  $^{116}\text{Xe}$  for the 1  $\mu\text{m}$  distance. The peaks from transitions in  $^{116}\text{Xe}$  that are visible in the spectrum are labeled. The spectrum results from a gate in detector ring 1 (forward angle) and also shows events from detector ring 1, so the shifted component of each peak has a higher energy than the unshifted component

and the mean recoil velocity  $v$  with the formula

$$\tau(x) = \frac{I_{\text{un}}}{v \cdot \frac{d}{dx} I_{\text{sh}}} \quad (1)$$

for a gate on a direct feeder. In case of a gate on an indirect feeder, i.e. a higher-lying transition that is not directly populating the level of interest, the intensity of the unshifted component has to be corrected for the direct feeder.

The recoil velocity  $v$  was determined from the energy shift between the shifted and unshifted peaks of different  $\gamma$ -ray transitions in  $^{116}\text{Xe}$ . From this a mean recoil velocity of  $v = 0.99(3) \% c$  was derived. The relative distances as well as the offset distance for absolute foil separation were determined with the capacitance method as first introduced by Alexander and Bell [51] and described in more detail in Ref. [52]. To correct for differences in beam intensity and run time between the different distance runs, a normalization factor was determined for every distance.

The gates were set separately for the two detector rings, since the gate has to be set on the shifted component and the energy shift depends on the detection angle. For every distance, this results in one spectrum for each of the four ring-ring combinations N\_M. To increase the statistics in the spectra, the two gated spectra of the same ring, i.e. spectra with same N, were summed into one spectrum. Thus, for each distance, two statistically independent spectra were used for the lifetime analysis. In Fig. 5 the evolution of the shifted and unshifted intensities of the  $2_1^+ \rightarrow 0_1^+$  transition can be seen for different distances.

For the DDCM analysis, the program Napatau [53] was used. In this program a lifetime curve is fitted simultaneously to the normalized intensities of the shifted and unshifted component, where the shifted component is described by continu-

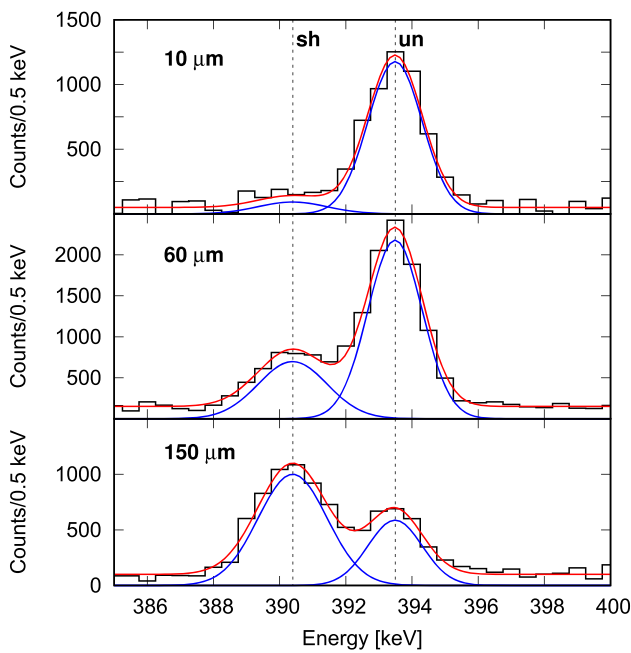


**Fig. 5** Fitted peaks of the shifted and unshifted component of the  $2_1^+ \rightarrow 0_1^+$  transition. The spectra are from detectors at  $142.3^\circ$  for distances 10, 60 and  $150\mu\text{m}$  gated on the shifted component of the  $4_1^+ \rightarrow 2_1^+$  transition. In blue the gaussian functions describing each respective peak are shown. The position and width of each function are held constant for all distances. In red the total fit functions are shown consisting of the sum of both peaks and a linear background function

ously connected second-order polynomials and the unshifted component is described by the derivative of these polynomials multiplied by a proportionality factor following Eq. (1). In this step, the proportionality factor is however only treated as a fit parameter of the curve and is not directly used to determine the lifetime. The lifetime is extracted in a second step for each distance separately using again Eq. (1) where for  $\frac{d}{dx} I_{\text{sh}}(x)$  the derivative of the polynomial fit function is used. The error calculation takes the covariance between the function  $I_{\text{sh}}(x)$  and the measured value  $I_{\text{un}}(x)$  into account. From all measurement points inside the sensitive region, where the derivative  $\frac{d}{dx} I_{\text{sh}}(x)$  is larger than half of its maximum value, the weighted average is taken as the resulting lifetime. Exemplary lifetime fits from Napatau for the  $2_1^+$  and  $4_1^+$  states can be seen in Figs. 6 and 7, respectively.

The lifetimes of the  $2_1^+$  and  $4_1^+$  states were determined using this method. For each of the states, results could be obtained using spectra from a gate on a direct feeder as well as an indirect feeder. Since the results from an indirect gate are dependent on data used also in the direct gate, the indirect gates were only used for a consistency check. The weighted average of the results from the direct gate from different detector rings is taken as the adopted lifetime value for each state as listed in Table 1. The results from the respective indirect gates are consistent within the uncertainty range.

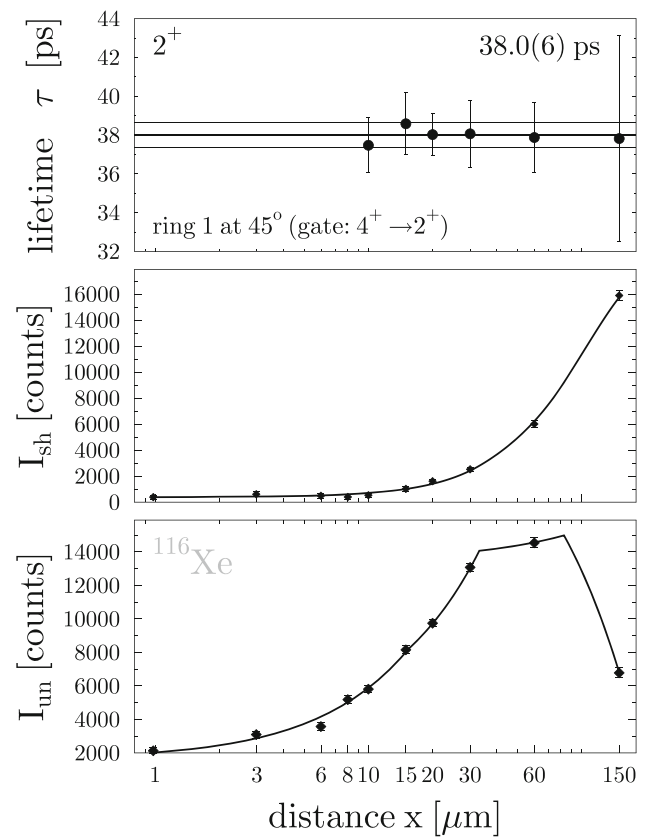


**Fig. 6** Exemplary lifetime curve fit from Napatau for the  $2_1^+$  state. From bottom to top, the intensities of the unshifted components, intensities of the shifted components and resulting lifetimes are shown. The lifetime value in the top-right corner is the weighted average of the values from the different distances

For the  $6_1^+$  and  $7_1^-$  states, lifetimes were at first also obtained in the same manner. However, the lifetimes resulting from the DDCM analysis for these states are of the order of the expected stopping time inside the stopper foil. Thus Doppler-shift attenuation effects have to be taken into account. When decays occur inside the stopper but before the nucleus is fully stopped, the  $\gamma$  energy is shifted but not as much as the fully shifted peak. When the stopping time is not negligible compared to the level lifetime, this leads to a deviation from the Gaussian shape of the  $\gamma$  peaks resulting in a wrong evaluation of the lifetime.

To evaluate the lifetimes of the short-lived  $6_1^+$  and  $7_1^-$  states, simulated spectra were used from the Geant4-based simulation code PTBG4 [54], which accounts for the stopping power of the stopper foil material. Input parameters of the code are positions, materials and thicknesses of the target and stopper foils, efficiency and positions of the detectors, material and energy of the beam and the simulated cascades of excited states with assumed lifetimes of the respective states. Unlike in the DDCM analysis, absolute target-to-stopper distances are needed. Reaction events with these

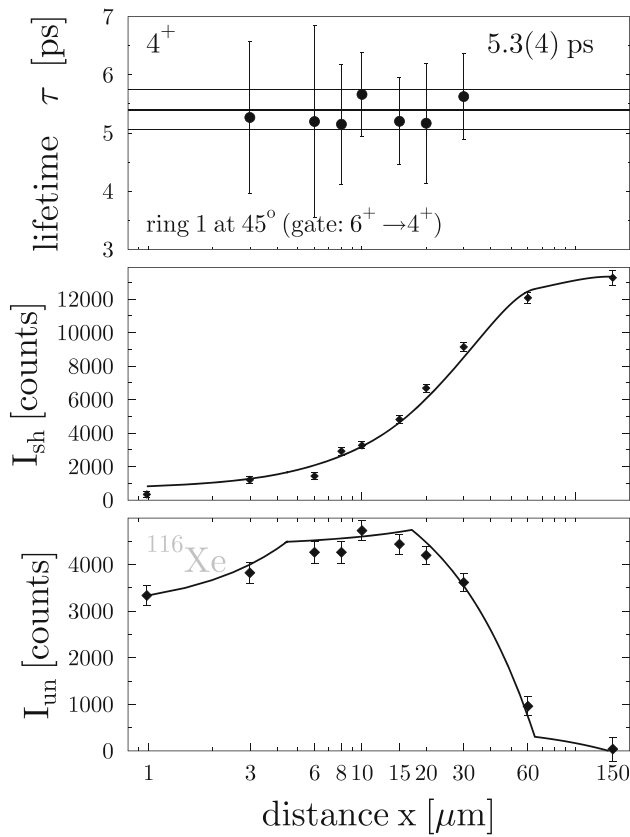


Fig. 7 Same as Fig. 6 but for the  $4_1^+$  state

parameters were simulated with the code and then sorted into  $\gamma$ - $\gamma$ -coincidence matrices similar to the experimental data. The simulation was repeated for various lifetimes of the level of interest. The level lifetime was then deduced from the minimization of

$$\chi^2 = \sum_{i=j}^k \left( \frac{n_{i,\text{exp}} - n_{i,\text{sim}}}{\Delta n_{i,\text{exp}}} \right)^2 \quad (2)$$

where  $n_{i,\text{exp/sim}}$  is the number of counts in the  $i$ -th bin of the experimental/simulated spectrum and the bins  $j$  to  $k$  are taken into account for the  $\chi^2$  minimization.

The relative intensities of the shifted and unshifted components in the resulting simulated spectra depend on the lifetime of the state of interest as well as the feeding conditions. In order to fix the feeding cascade and make a comparison to the experimental spectra possible, a gate was set on the shifted component of a feeding transition in the simulated matrices and the exact same gate was set in the matrices from the experimental data. To simplify the feeding conditions in the simulation, an effective lifetime was simulated as the lifetime of the feeder on which the gate was set. The effective lifetime of the feeding state was obtained from the experimental data prior to running the simulation by gating

Table 1 Lifetime results of the DDCM analysis for the  $2_1^+$  and  $4_1^+$  states

State	Source	$\tau$ [ps]
$2_1^+$	det. ring 1	38.0 (6)
	det. ring 2	37.9 (6)
	Adopted value	38.0 (4)
	lit. value [2]	35.1 (13)
$4_1^+$	det. ring 1	5.3 (4)
	det. ring 2	5.5 (3)
	Adopted value	5.4 (2)
	lit. value [2]	4.8 (2)

Table 2 Lifetime results for the  $6_1^+$  and  $7_1^-$  states from the DDCM analysis as well as from the simulations. Note that the results from the DDCM analysis of the  $6_1^+$  and  $7_1^-$  states were not taken for the final results. See text for detail

State	Source	$\tau$ [ps]
$6_1^+$	DDCM	1.4 (9)
	Simulation	3.3 (10)
	lit. value [2]	2.4 (2)
$7_1^-$	DDCM	0.7 (5)
	Simulation	2.3 (10)
	lit. value [2]	3.0 (12)

from below and extracting  $\tau$  from the decay equation

$$R(x) = \frac{I_{\text{un}}(x)}{I_{\text{un}}(x) + I_{\text{sh}}(x)} = \exp\left(\frac{-x}{v \cdot \tau}\right). \quad (3)$$

This simulation was performed for the  $6_1^+$  and  $7_1^-$  lifetime separately with the  $7_1^-$  and  $9_1^-$  as simulated feeder, respectively. The uncertainty of the results was estimated by the variation between the results from different spectra and by varying the most crucial input parameters of the simulation inside their uncertainty range. In Fig. 8 the experimental spectrum from detector ring 1 for the 15  $\mu\text{m}$  distance showing the  $7_1^- \rightarrow 6_1^+$  transition and the respective spectrum simulated for lifetimes of  $\tau(7_1^-) = 0.7, 2.3$  and 5.0 ps are shown. The respective  $\chi^2$  distribution is also shown in the inset. The results of the simulations are listed in Table 2 together with the results from the DDCM analysis.

The adopted lifetime values for all states are listed again in Table 3 together with the respective reduced transition strengths.

### 4 Conclusion

In summary, reliable lifetimes of the  $2_1^+, 4_1^+, 6_1^+$  and  $7_1^-$  states in  $^{116}\text{Xe}$  were measured and the resulting reduced transition strengths were determined. The lifetime values of the

**Table 3** Final lifetime results and extracted reduced transition strengths

$J^\pi$	$\tau(J^\pi)$ [ps]	$J^\pi \rightarrow J_f^\pi$	$E_\gamma$ [keV]	$EL$	Branching ratio	$B(E_L; J^\pi \rightarrow J_f^\pi)[e^2\text{fm}^{2L}]$
$2^+$	38.0 (4)	$2^+ \rightarrow 0^+$	393.6	E2	1.0	$2230 \pm 20$
$4^+$	5.4 (2)	$4^+ \rightarrow 2^+$	524.3	E2	1.0	$3790^{+150}_{-140}$
$6^+$	3.3 (10)	$6^+ \rightarrow 4^+$	615.1	E2	1.0	$2800^{+1200}_{-700}$
$7^-$	2.3 (10)	$7^- \rightarrow 5^-$	465.2	E2	0.22 (8) [2]	$3500^{+2900}_{-1400}$
		$7^- \rightarrow 6^+$	911.6	E1	0.78 (8) [2]	$2.8^{+2.1}_{-0.9} \cdot 10^{-4}$

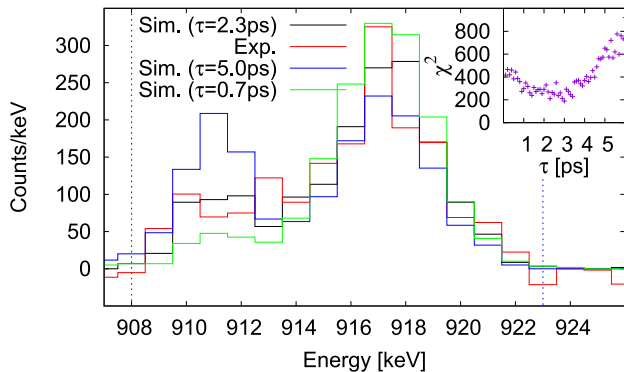


**Fig. 8** Experimental spectrum of the  $7_1^- \rightarrow 6_1^+$  transition for detectors at  $45^\circ$  in comparison to the respective spectra simulated for lifetimes of  $\tau(7_1^-) = 0.7, 2.3, 5.0$  ps. The spectra correspond to the  $15 \mu\text{m}$  distance with a gate on the shifted component of the  $9_1^- \rightarrow 7_1^-$  transition. The experimental spectrum is corrected for background with a linear function. The region considered in the  $\chi^2$  minimization is marked with blue lines. The spectra are normalized, so that the number of counts in the considered region is equal. The inset shows the  $\chi^2$  distribution for different simulated lifetimes of the  $7_1^-$  state

$6_1^+$  and  $7_1^-$  states previously measured in Ref. [2] could be confirmed within the margin of uncertainty. The relatively large  $B(E1; 7_1^- \rightarrow 6_1^+)$  value suggests a discussion in the framework of octupole correlations, considering the exceptionally large E3 transition strengths of  $B(E3) \approx 70$  W.u. that have been measured in neighboring  $^{114}\text{Xe}$  [3]. However, no E3 transitions are known in  $^{116}\text{Xe}$ , which would be a crucial indicator for the investigation of octupole correlations. Furthermore, calculations from Nomura et al. [55] suggest octupole deformations only in the very neutron-deficient Xe isotopes with  $A \approx 108 - 112$ , while for  $^{116}\text{Xe}$  a pronounced quadrupole collectivity is suggested.

The lifetime results of the  $2_1^+$  and  $4_1^+$  states are only overlapping with the values previously measured in Ref. [2] within the  $2\sigma$  range. One possible explanation for this could be errors in the accounting for the complex feeding conditions in the calculations of lifetimes in Ref. [2]. In this work the lifetimes of the  $2_1^+$  and  $4_1^+$  states were determined using the DDCM in  $\gamma$ - $\gamma$ -coincidence mode avoiding the need for any feeding assumptions for the first time. However, the  $B_{4/2} = 1.70(7)$  ratio extracted from this work confirms the

value from Ref. [2] and thus the sharp drop in transition strength of the  $4_1^+ \rightarrow 2_1^+$  transition between  $^{116}\text{Xe}$  and  $^{114}\text{Xe}$ . While the cause for this lowering of  $B_{4/2}$  ratios remains unexplained, this strengthens the picture of a very abrupt change in  $B(E2; 4_1^+ \rightarrow 2_1^+)$  transition strengths that is seen in the Sn, Te and Xe isotopic chains and suggests a connection between these.

Further investigations on transition strengths in this region are needed to enhance the picture, especially in more neutron-deficient Xe isotopes and  $^{116}\text{Te}$ . For the latter, the determination of a  $B_{4/2}$  ratio is difficult due to the fact that the  $4_1^+ \rightarrow 2_1^+$  and  $2_1^+ \rightarrow 0_1^+$  transitions form a doublet. The lighter ( $A \leq 114$ ) Xe isotopes on the other hand are difficult to reach experimentally since they are very far away from the valley of stability and can thus only be produced with very low cross sections or from radioactive ion beams.

To explain the general structure in this region and the evolution of transition strengths in particular, an extension of the aforementioned Monte Carlo shell model calculations from Togashi et al. [48] to the neighboring Te and Xe isotopic chains, especially including transition strengths for the  $2^+$  and  $4^+$  yrast states, would be highly desirable. These calculations were done in Ref. [48] for the  $2_1^+$  states in Sn isotopes solely. This extension could provide a fundamental understanding of the structural evolution from “regular” collectivity of the lowest states towards  $B_{4/2} < 1$  that cannot be understood so far.

**Acknowledgements** This work was supported by the Deutsche Forschungsgemeinschaft (DFG) under Contract No. FR 3276/2-1 and DE 1516/5-1. We further acknowledge funding from the DFG for the upgrade of the Cologne Germanium detector array under Grant INST 216/988-1 FUGG.

**Funding** Open Access funding enabled and organized by Projekt DEAL.

**Data Availability Statement** The datasets generated and analysed during the current study are available from the corresponding author on reasonable request.

**Open Access** This article is licensed under a Creative Commons Attribution 4.0 International License, which permits use, sharing, adaptation, distribution and reproduction in any medium or format, as long as you give appropriate credit to the original author(s) and the source, provide a link to the Creative Commons licence, and indicate if changes

were made. The images or other third party material in this article are included in the article's Creative Commons licence, unless indicated otherwise in a credit line to the material. If material is not included in the article's Creative Commons licence and your intended use is not permitted by statutory regulation or exceeds the permitted use, you will need to obtain permission directly from the copyright holder. To view a copy of this licence, visit <http://creativecommons.org/licenses/by/4.0/>.

## References

1. R. Casten,  $N_p N_n$  systematics in heavy nuclei. Nucl. Phys. A **443**(1), 1–28 (1985). [https://doi.org/10.1016/0375-9474\(85\)90318-5](https://doi.org/10.1016/0375-9474(85)90318-5)
2. J. DeGraaf, M. Cromaz, T.E. Drake, V.P. Janzen, D.C. Radford, D. Ward, Lifetime measurements in  $^{114,116}\text{Xe}$  isotopes. Phys. Rev. C **58**, 164–171 (1998). <https://doi.org/10.1103/PhysRevC.58.164>
3. G. de Angelis, A. Gadea, E. Farnea, R. Isocrate, P. Petkov, N. Marginean, D. Napoli, A. Dewald, M. Bellato, A. Bracco, F. Camera, D. Curien, M. De Poli, E. Fioretto, A. Fitzler, S. Kasemann, N. Kintz, T. Klug, S. Lenzi, S. Lunardi, R. Menegazzo, P. Pavan, J. Pedroza, V. Pucknell, C. Ring, J. Sampson, R. Wyss, Coherent proton-neutron contribution to octupole correlations in the neutron-deficient  $^{114}\text{Xe}$  nucleus. Phys. Lett. B **535**(1), 93–102 (2002). [https://doi.org/10.1016/S0370-2693\(02\)01728-8](https://doi.org/10.1016/S0370-2693(02)01728-8). <https://www.sciencedirect.com/science/article/pii/S0370269302017288>
4. O. Möller, N. Warr, J. Jolie, A. Dewald, A. Fitzler, A. Linnemann, K.O. Zell, P.E. Garrett, S.W. Yates, E2 transition probabilities in  $^{114}\text{Te}$ : a conundrum. Phys. Rev. C **71**, 064324 (2005). <https://doi.org/10.1103/PhysRevC.71.064324>
5. C. Müller-Gatermann, A. Dewald, C. Fransen, M. Beckers, A. Blazhev, T. Braunroth, A. Goldkuhle, J. Jolie, L. Kornwebel, W. Reviol, F. von Spee, K.O. Zell, Evolution of collectivity in  $^{118}\text{Xe}$ . Phys. Rev. C **102**, 064318 (2020). <https://doi.org/10.1103/PhysRevC.102.064318>
6. T. Bäck, C. Qi, F. Ghazi Moradi, B. Cederwall, A. Johnson, R. Liotta, R. Wyss, H. Al-Azri, D. Bloor, T. Brock, R. Wadsworth, T. Grahn, P.T. Greenlees, K. Hauschild, A. Herzán, U. Jakobsson, P.M. Jones, R. Julin, S. Juutinen, S. Ketelhut, M. Leino, A. Lopez-Martens, P. Nieminen, P. Peura, P. Rahkila, S. Rinta-Antila, P. Ruotsalainen, M. Sandzelius, J. Sarén, C. Scholey, J. Sorri, J. Uusitalo, S. Go, E. Ideguchi, D.M. Cullen, M.G. Procter, T. Braunroth, A. Dewald, C. Fransen, M. Hackstein, J. Litzinger, W. Rother, Lifetime measurement of the first excited  $2^+$  state in  $^{108}\text{Te}$ . Phys. Rev. C **84**, 041306 (2011). <https://doi.org/10.1103/PhysRevC.84.041306>
7. D.A. Testov, S. Bakes, J.J. Valiente-Dobón, A. Goasduff, S. Frauendorf, F. Nowacki, T.R. Rodríguez, G. de Angelis, D. Bazzacco, C. Boiano, A. Boso, B. Cederwall, M. Cicerchia, P. Čolović, G. Colucci, F. Didierjean, M. Doncel, J.A. Dueñas, F. Galtarossa, A. Gozzelino, K. Hadyńska-Kleń, G. Jaworski, P.R. John, S. Lenzi, H. Liu, S. Lunardi, R. Menegazzo, D. Mengoni, A. Mentana, D.R. Napoli, G. Pasqualato, F. Recchia, S. Riccetto, L.M. Robledo, M. Rocchini, B. Saygi, M. Siciliano, Y. Sobolev, S. Szilner, Octupole correlations near  $^{110}\text{Te}$ . Phys. Rev. C **103**, 044321 (2021). <https://doi.org/10.1103/PhysRevC.103.044321>
8. M. Doncel, T. Bäck, D.M. Cullen, D. Hodge, C. Qi, B. Cederwall, M.J. Taylor, M. Procter, K. Auranen, T. Grahn, P.T. Greenlees, U. Jakobsson, R. Julin, S. Juutinen, A. Herzán, J. Konki, M. Leino, J. Pakarinen, J. Partanen, P. Peura, P. Rahkila, P. Ruotsalainen, M. Sandzelius, J. Sarén, C. Scholey, J. Sorri, S. Stolze, J. Uusitalo, Lifetime measurement of the first excited  $2^+$  state in  $^{112}\text{Te}$ . Phys. Rev. C **91**, 061304 (2015). <https://doi.org/10.1103/PhysRevC.91.061304>
9. A. Pasternak, J. Srebrny, A. Efimov, V. Mikhajlov, E. Podsvirova, C. Droste, T. Morek, S. Juutinen, G. Hagemann, M. Piiparinen, S. Törmänen, A. Virtanen, Lifetimes in the ground-state band and the structure of  $^{118}\text{Te}$ . Eur. Phys. J. A **13**, 435 (2002). <https://doi.org/10.1140/epja/iepja1221>
10. M. Saxena, R. Kumar, A. Jhingan, S. Mandal, A. Stolarz, A. Banerjee, R.K. Bhowmik, S. Dutt, J. Kaur, V. Kumar, M. Modou Mbaye, V.R. Sharma, H.J. Wollersheim, Rotational behavior of  $^{120,122,124}\text{Te}$ . Phys. Rev. C **90**, 024316 (2014). <https://doi.org/10.1103/PhysRevC.90.024316>
11. A. Bockisch, A. Kleinfeld, Reorientation effect measurements of  $^{122}\text{Te}$  and  $^{130}\text{Te}$ . Nucl. Phys. A **261**(3), 498–510 (1976). [https://doi.org/10.1016/0375-9474\(76\)90163-9](https://doi.org/10.1016/0375-9474(76)90163-9). <https://www.sciencedirect.com/science/article/pii/0375947476901639>
12. S.F. Hicks, G.K. Alexander, C.A. Aubin, M.C. Burns, C.J. Collard, M.M. Walbran, J.R. Vanhoy, E. Jensen, P.E. Garrett, M. Kadi, A. Martin, N. Warr, S.W. Yates, Intruder structures observed in  $^{122}\text{Te}$  through inelastic neutron scattering. Phys. Rev. C **71**, 034307 (2005). <https://doi.org/10.1103/PhysRevC.71.034307>
13. J. Barrette, M. Barrette, R. Haroutunian, G. Lamoureux, S. Monaro, Investigation of the reorientation effect on  $^{122}\text{Te}$ ,  $^{124}\text{Te}$ ,  $^{126}\text{Te}$ ,  $^{128}\text{Te}$ , and  $^{130}\text{Te}$ . Phys. Rev. C **10**, 1166–1171 (1974). <https://doi.org/10.1103/PhysRevC.10.1166>
14. M.J. Bechara, O. Dietzsch, M. Samuel, U. Smilansky, Reorientation effect measurements in  $^{122}\text{Te}$  and  $^{128}\text{Te}$ . Phys. Rev. C **17**, 628–633 (1978). <https://doi.org/10.1103/PhysRevC.17.628>
15. M. Samuel, U. Smilansky, B. Watson, Y. Eisen, A. Kleinfeld, D. Werdecker, Measurement of nuclear deformation parameters from elastic and inelastic scattering of  $\alpha$  and  $^3\text{He}$  ions on Te isotopes. Nucl. Phys. A **279**(2), 210–222 (1977). [https://doi.org/10.1016/0375-9474\(77\)90224-X](https://doi.org/10.1016/0375-9474(77)90224-X). <https://www.sciencedirect.com/science/article/pii/037594747790224X>
16. S. Vasconcelos, M. Rao, N. Ueta, C. Appoloni, Coulomb-nuclear interference in the scattering of  $^3\text{He}$  and  $\alpha$ -particles by  $^{122,124}\text{Te}$ ,  $^{124}\text{Sn}$  and  $^{114}\text{Cd}$ . Nucl. Phys. A **313**(3), 333–345 (1979). [https://doi.org/10.1016/0375-9474\(79\)90504-9](https://doi.org/10.1016/0375-9474(79)90504-9). <https://www.sciencedirect.com/science/article/pii/0375947479905049>
17. A. Kleinfeld, G. Mäggi, D. Werdecker, Reorientation effect measurements in  $^{124}\text{Te}$ ,  $^{126}\text{Te}$  and  $^{128}\text{Te}$ . Nucl. Phys. A **248**(2), 342–355 (1975). [https://doi.org/10.1016/0375-9474\(75\)90169-4](https://doi.org/10.1016/0375-9474(75)90169-4). <https://www.sciencedirect.com/science/article/pii/0375947475901694>
18. A.E. Stuchbery, J.M. Allmond, A. Galindo-Uribarri, E. Padilla-Rodal, D.C. Radford, N.J. Stone, J.C. Batchelder, J.R. Beene, N. Benczer-Koller, C.R. Bingham, M.E. Howard, G.J. Kumbartzki, J.F. Liang, B. Manning, D.W. Stracener, C.H. Yu, Electromagnetic properties of the  $2_1^+$  state in  $^{134}\text{Te}$ : influence of core excitation on single-particle orbits beyond  $^{132}\text{Sn}$ . Phys. Rev. C **88**, 051304 (2013). <https://doi.org/10.1103/PhysRevC.88.051304>
19. D. Kumar, T. Bhattacharjee, S.S. Alam, S. Basak, L. Gerhard, L. Knafla, A. Esmaylzadeh, M. Ley, F. Dunkel, K. Schomaker, J.M. Régis, J. Jolie, Y.H. Kim, U. Köster, G.S. Simpson, L.M. Fraile, Lifetimes and transition probabilities for low-lying yrast levels in  $^{130,132}\text{Te}$ . Phys. Rev. C **106**, 034306 (2022). <https://doi.org/10.1103/PhysRevC.106.034306>
20. C. Barton, M. Caprio, D. Shapira, N. Zamfir, D. Brenner, R. Gill, T. Lewis, J. Cooper, R. Casten, C. Beausang, R. Krücken, J. Novak, B(E2) values from low-energy Coulomb excitation at an ISOL facility: the  $N=80,82$  Te isotopes. Phys. Lett. B **551**(3), 269–276 (2003). [https://doi.org/10.1016/S0370-2693\(02\)03066-6](https://doi.org/10.1016/S0370-2693(02)03066-6). <https://www.sciencedirect.com/science/article/pii/S0370269302030666>
21. M. Danchev, G. Rainovski, N. Pietralla, A. Gargano, A. Covello, C. Baktash, J.R. Beene, C.R. Bingham, A. Galindo-Uribarri, K.A. Gladnishki, C.J. Gross, V.Y. Ponomarev, D.C. Radford, L.L. Riedinger, M. Scheck, A.E. Stuchbery, J. Wambach, C.H. Yu, N.V. Zamfir, One-phonon isovector  $2_{1,MS}^+$  state in the neutron-rich nucleus  $^{132}\text{Te}$ . Phys. Rev. C **84**, 061306 (2011). <https://doi.org/10.1103/PhysRevC.84.061306>

22. I.M. Govil, A. Kumar, H. Iyer, P. Joshi, S.K. Chamoli, R. Kumar, R.P. Singh, U. Garg, Recoil distance lifetime measurements in  $^{118}\text{Xe}$ . *Phys. Rev. C* **66**, 064318 (2002). <https://doi.org/10.1103/PhysRevC.66.064318>
23. J.C. Walpe, B.F. Davis, S. Naguleswaran, W. Reviol, U. Garg, X.W. Pan, D.H. Feng, J.X. Saladin, Lifetime measurements in  $^{120}\text{Xe}$ . *Phys. Rev. C* **52**, 1792–1795 (1995). <https://doi.org/10.1103/PhysRevC.52.1792>
24. W. Kutschera, W. Dehnhardt, O.C. Kistner, P. Kump, B. Povh, H.J. Sann, Lifetime measurements in  $^{120,122}\text{Xe}$  and  $^{126,128}\text{Ba}$ . *Phys. Rev. C* **5**, 1658–1662 (1972). <https://doi.org/10.1103/PhysRevC.5.1658>
25. C. Droste, T. Morek, S.G. Rohozinski, D. Alber, H. Grawe, D. Chlebowska, Lifetimes in  $^{121,123}\text{Cs}$  and the question of core stiffness. *J. Phys. G: Nucl. Part. Phys.* **18**(11), 1763 (1992). <https://doi.org/10.1088/0954-3899/18/11/009>
26. I.M. Govil, A. Kumar, H. Iyer, H. Li, U. Garg, S.S. Ghugre, T. Johnson, R. Kaczarowski, B. Kharraja, S. Naguleswaran, J.C. Walpe, Recoil distance lifetime measurements in  $^{122,124}\text{Xe}$ . *Phys. Rev. C* **57**, 632–636 (1998). <https://doi.org/10.1103/PhysRevC.57.632>
27. P. Petkov, R. Krücken, A. Dewald, P. Sala, G. Böhm, J. Altmann, A. Gelberg, P. von Brentano, R. Jolie, W. Andrejtschegg, RDDS measurements of collective E2 transition strengths in  $^{122}\text{Xe}$ . *Nucl. Phys. A* **568**(3), 572–600 (1994). [https://doi.org/10.1016/0375-9474\(94\)90395-6](https://doi.org/10.1016/0375-9474(94)90395-6). <https://www.sciencedirect.com/science/article/pii/0375947494903956>
28. B. Saha, A. Dewald, O. Möller, R. Peusquens, K. Jessen, A. Fitzler, T. Klug, D. Tonev, P. Brentano, J. Jolie, B.J.P. Gall, P. Petkov, Probing nuclear structure of  $^{124}\text{Xe}$ . *Phys. Rev. C* **70**, 034313 (2004). <https://doi.org/10.1103/PhysRevC.70.034313>
29. W.F. Mueller, M.P. Carpenter, J.A. Church, D.C. Dinca, A. Gade, T. Glasmacher, D.T. Henderson, Z. Hu, R.V.F. Janssens, A.F. Lisetskiy, C.J. Lister, E.F. Moore, T.O. Pennington, B.C. Perry, I. Wiedenhöver, K.L. Yurkewicz, V.G. Zelevinsky, H. Zwahlen, Variation with mass of  $B(E3; 0_1^+ \rightarrow 3_1^-)$  transition rates in  $A = 124 - 134$  even-mass xenon nuclei. *Phys. Rev. C* **73**, 014316 (2006). <https://doi.org/10.1103/PhysRevC.73.014316>
30. G. Rainovski, N. Pietralla, T. Ahn, L. Coquard, C. Lister, R. Janssens, M. Carpenter, S. Zhu, L. Bettermann, J. Jolie, W. Rother, R. Jolos, V. Werner, How close to the O(6) symmetry is the nucleus  $^{124}\text{Xe}$ ? *Phys. Lett. B* **683**(1), 11–16 (2010). <https://doi.org/10.1016/j.physletb.2009.12.007>. <https://www.sciencedirect.com/science/article/pii/S0370269309014294>
31. A. Chester, P. Adrich, A. Becerril, D. Bazin, C. Campbell, J. Cook, D.C. Dinca, W. Mueller, D. Miller, V. Moeller, R. Norris, M. Portillo, K. Starosta, A. Stolz, J. Terry, H. Zwahlen, C. Vaman, A. Dewald, Application of the time-of-flight technique for lifetime measurements with relativistic beams of heavy nuclei. *Nucl. Inst. Meth. A* **562**(1), 230–240 (2006). <https://doi.org/10.1016/j.nima.2006.02.182>. <https://www.sciencedirect.com/science/article/pii/S0168900206004748>
32. D.M. Gordon, L.S. Eytel, H. de Waard, D.E. Murnick, Perturbed-angular-correlation studies of  $2^+$  levels of even xenon isotopes. *Phys. Rev. C* **12**, 628–636 (1975). <https://doi.org/10.1103/PhysRevC.12.628>
33. E. Clément, A. Lemasson, M. Rejmund, B. Jacquot, D. Ralet, C. Michelagnoli, D. Barrientos, P. Bednarczyk, G. Benzoni, A.J. Boston, A. Bracco, B. Cederwall, M. Ciemala, J. Collado, F. Crespi, C. Domingo-Pardo, J. Dudouet, H.J. Eberth, G. de France, A. Gadea, V. Gonzalez, A. Gottardo, L. Harkness, H. Hess, A. Jungclauss, A. Kaşkaş, W. Korten, S.M. Lenzi, S. Leoni, J. Ljungvall, R. Menegazzo, D. Mengoni, B. Million, D.R. Napoli, J. Nyberg, Z. Podolyak, A. Pullia, B. Quintana Arnés, F. Recchia, N. Redon, P. Reiter, M. D.Salsac, E. Sanchis, M. Şenyiğit, M. Siciliano, D. Sohler, O. Stezowski, C. Theisen, J.J. Valiente Dobón, Spectroscopic quadrupole moments in  $^{124}\text{Xe}$ . *Phys. Rev. C* **107**, 014324 (2023). <https://doi.org/10.1103/PhysRevC.107.014324>
34. J. Srebrny, T. Czosnyka, W. Karczmarczyk, P. Napiorkowski, C. Droste, H.J. Wollersheim, H. Emling, H. Grein, R. Kulesa, D. Cline, C. Fahlander, E1, E2, E3 and M1 information from heavy ion coulomb excitation. *Nucl. Phys. A* **557**, 663–672 (1993). [https://doi.org/10.1016/0375-9474\(93\)90578-L](https://doi.org/10.1016/0375-9474(93)90578-L). <https://www.sciencedirect.com/science/article/pii/037594749390578L>
35. W. Rother, A. Dewald, G. Pascovici, C. Fransen, G. Frießner, M. Hackstein, G. Ilie, H. Iwasaki, J. Jolie, B. Melon, P. Petkov, M. Pfeiffer, T. Pissulla, K.O. Zell, U. Jakobsson, R. Julin, P. Jones, S. Ketelhut, P. Nieminen, P. Peura, P. Rähkila, J. Uusitalo, C. Scholey, S. Harissopoulos, A. Lagoyannis, T. Konstantinopoulos, T. Grahn, D. Balabanski, A new recoil distance technique using low energy coulomb excitation in inverse kinematics. *Nucl. Instrum. Methods. A* **654**(1), 196–205 (2011). <https://doi.org/10.1016/j.nima.2011.05.075>. <https://www.sciencedirect.com/science/article/pii/S0168900211011090>
36. J. Burde, S. Eshhar, A. Ginzburg, E. Navon, Absolute transition probabilities in  $^{130}\text{Xe}$ . *Nucl. Phys. A* **229**(3), 387–396 (1974). [https://doi.org/10.1016/0375-9474\(74\)90659-9](https://doi.org/10.1016/0375-9474(74)90659-9). <https://www.sciencedirect.com/science/article/pii/0375947474906599>
37. P.F. Kenealy, G.B. Beard, K. Parsons, Nuclear-resonance fluorescence in  $\text{Xe}^{130}$ . *Phys. Rev. C* **2**, 2009–2015 (1970). <https://doi.org/10.1103/PhysRevC.2.2009>
38. G. Jakob, N. Benczer-Koller, G. Kumbartzki, J. Holden, T.J. Mertzimekis, K.H. Speidel, R. Ernst, A.E. Stuchbery, A. Pakou, P. Maier-Komor, A. Macchiavelli, M. McMahan, L. Phair, I.Y. Lee, Evidence for proton excitations in  $^{130,132,134,136}\text{Xe}$  isotopes from measurements of  $g$  factors of  $2_1^+$  and  $4_1^+$  states. *Phys. Rev. C* **65**, 024316 (2002). <https://doi.org/10.1103/PhysRevC.65.024316>
39. L. Morrison, K. Hadyńska-Klęk, Z. Podolyák, D.T. Doherty, L.P. Gaffney, L. Kaya, L. Próchniak, J. Samorajczyk-Pyśk, J. Srebrny, T. Berry, A. Boukhari, M. Brunet, R. Canavan, R. Catherall, S.J. Colosimo, J.G. Cubiss, H. De Witte, C. Fransen, E. Giannopoulos, H. Hess, T. Kröll, N. Lalović, B. Marsh, Y.M. Palenzuela, P.J. Napiorkowski, G. O'Neill, J. Pakarinen, J.P. Ramos, P. Reiter, J.A. Rodriguez, D. Rosiak, S. Rothe, M. Rudigier, M. Siciliano, J. Snäll, P. Spagnoletti, S. Thiel, N. Warr, F. Wenander, R. Zidarova, M. Zielińska, Quadrupole deformation of  $^{130}\text{Xe}$  measured in a coulomb-excitation experiment. *Phys. Rev. C* **102**, 054304 (2020). <https://doi.org/10.1103/PhysRevC.102.054304>
40. W.D. Hamilton, The lifetime of the 673 keV level in  $^{132}\text{Xe}$ . *Proc. Phys. Soc.* **78**(5), 1064 (1961). <https://doi.org/10.1088/0370-1328/78/5/354>
41. S.S. Alam, T. Bhattacharjee, D. Banerjee, A. Saha, S. Das, M.S. Sarkar, S. Sarkar, Lifetimes and transition probabilities for the low-lying states in  $^{131}\text{I}$  and  $^{132}\text{Xe}$ . *Phys. Rev. C* **99**, 014306 (2019). <https://doi.org/10.1103/PhysRevC.99.014306>
42. E.E. Peters, A. Chakraborty, B.P. Crider, S.F. Ashley, E. Elhami, S.F. Hicks, A. Kumar, M.T. McEllistrem, S. Mukhopadhyay, J.N. Orce, F.M. Prados-Estévez, S.W. Yates, Level lifetimes and the structure of  $^{134}\text{Xe}$  from inelastic neutron scattering. *Phys. Rev. C* **96**, 014313 (2017). <https://doi.org/10.1103/PhysRevC.96.014313>
43. H. von Garrel, P.v. Brentano, C. Fransen, G. Friessner, N. Hollmann, J. Jolie, F. Käppeler, L. Käubler, U. Kneissl, C. Hohstall, L. Kostov, A. Linnemann, D. MÜcher, N. Pietralla, H.H. Pitz, G. Rusev, M. Scheck, K.D. Schilling, C. Scholl, R. Schwengner, F. Stedile, S. Walter, V. Werner, K. Wisshak, Low-lying  $E1$ ,  $M1$ , and  $E2$  strength distributions in  $^{124,126,128,129,130,131,132,134,136}\text{Xe}$ : systematic photon scattering experiments in the mass region of a nuclear shape or phase transition. *Phys. Rev. C* **73**, 054315 (2006). <https://doi.org/10.1103/PhysRevC.73.054315>
44. K. Speidel, H. Busch, S. Kremeyer, U. Knopp, J. Cub, M. Busas, W. Karle, K. Freitag, U. Grabow, J. Gerber, Measurements of magnetic moments of  $^{134,136}\text{Xe}(2_1^+)$  and the mean life of the

- $^{136}\text{Xe}(2_1^+)$  state. Nucl. Phys. A **552**(1), 140–148 (1993). [https://doi.org/10.1016/0375-9474\(93\)90336-V](https://doi.org/10.1016/0375-9474(93)90336-V). <https://www.sciencedirect.com/science/article/pii/037594749390336V>
45. R.B. Cakirli, R.F. Casten, J. Jolie, N. Warr, Highly anomalous yrast  $B(E2)$  values and vibrational collectivity. Phys. Rev. C **70**, 047302 (2004). <https://doi.org/10.1103/PhysRevC.70.047302>
  46. T. Grahn, S. Stolze, D.T. Joss, R.D. Page, B. Saygi, D. O'Donnell, M. Akmalı, K. Andgren, L. Bianco, D.M. Cullen, A. Dewald, P.T. Greenlees, K. Heyde, H. Iwasaki, U. Jakobsson, P. Jones, D.S. Judson, R. Julin, S. Juutinen, S. Ketelhut, M. Leino, N. Lumley, P.J.R. Mason, O. Möller, K. Nomura, M. Nyman, A. Petts, P. Peura, N. Pietralla, T. Pissulla, P. Rahkila, P.J. Sappale, J. Sarén, C. Scholey, J. Simpson, J. Sorri, P.D. Stevenson, J. Uusitalo, H.V. Watkins, J.L. Wood, Excited states and reduced transition probabilities in  $^{168}\text{Os}$ . Phys. Rev. C **94**, 044327 (2016). <https://doi.org/10.1103/PhysRevC.94.044327>
  47. M. Doncel, T. Bäck, C. Qi, D.M. Cullen, D. Hodge, B. Cederwall, M.J. Taylor, M. Procter, M. Giles, K. Auranen, T. Grahn, P.T. Greenlees, U. Jakobsson, R. Julin, S. Juutinen, A. Herzáň, J. Konki, J. Pakarinen, J. Partanen, P. Peura, P. Rahkila, P. Ruotsalainen, M. Sandzelius, J. Sarén, C. Scholey, J. Sorri, S. Stolze, J. Uusitalo, Spin-dependent evolution of collectivity in  $^{112}\text{Te}$ . Phys. Rev. C **96**, 051304 (2017). <https://doi.org/10.1103/PhysRevC.96.051304>
  48. T. Togashi, Y. Tsunoda, T. Otsuka, N. Shimizu, M. Honma, Novel shape evolution in Sn isotopes from magic numbers 50 to 82. Phys. Rev. Lett. **121**, 062501 (2018). <https://doi.org/10.1103/PhysRevLett.121.062501>
  49. A. Dewald, O. Möller, P. Petkov, Developing the recoil distance doppler-shift technique towards a versatile tool for lifetime measurements of excited nuclear states. Prog. Part. Nucl. Phys. **67**(3), 786–839 (2012). <https://doi.org/10.1016/j.pnpnp.2012.03.003>. <https://www.sciencedirect.com/science/article/pii/S0146641012000713>
  50. N. Saed-Samii, A. Harter. SocoV2. <https://gitlab.ikp.uni-koeln.de/nima/soco-v2>
  51. T. Alexander, A. Bell, A target chamber for recoil-distance lifetime measurements. Nucl. Instrum. Methods **81**(1), 22–26 (1970). [https://doi.org/10.1016/0029-554X\(70\)90604-X](https://doi.org/10.1016/0029-554X(70)90604-X). <https://www.sciencedirect.com/science/article/pii/0029554X7090604X>
  52. M. Beckers, A. Dewald, C. Fransen, L. Kornweibel, C.D. Lakenbrink, F. von Spee, Revisiting the measurement of absolute foil-separation for RDDS measurements and introduction of an optical measurement method. Nucl. Instrum. Methods. A **1042**, 167416 (2022). <https://doi.org/10.1016/j.nima.2022.167416>. <https://www.sciencedirect.com/science/article/pii/S0168900222007082>
  53. B. Saha, Bestimmung der Lebensdauern kollektiver Kernanregungen in  $^{124}\text{Xe}$  und Entwicklung von entsprechender Analysesoftware. Ph.D. thesis, Universität zu Köln (2004)
  54. T. Braunroth. PTB Geant4. (**unpublished**)
  55. K. Nomura, R. Rodríguez-Guzmán, L.M. Robledo, Quadrupole-octupole coupling and the evolution of collectivity in neutron-deficient Xe, Ba, Ce, and Nd isotopes. Phys. Rev. C **104**, 054320 (2021). <https://doi.org/10.1103/PhysRevC.104.054320>